

# Fusion of OBD and GNSS Measurements of Speed

Johan Wahlström, Isaac Skog, *Senior Member, IEEE*,  
Robin Larsson Nordström, and Peter Händel, *Senior Member, IEEE*

**Abstract**—There are two primary sources of sensor measurements for driver behavior profiling within insurance telematics and fleet management. The first is the on-board diagnostics system, typically found within most modern cars. The second is the global navigation satellite system, whose associated receivers commonly are embedded into smartphones or off-the-shelf telematics devices. In this study, we present maximum likelihood and maximum a posteriori estimators for the problem of fusing speed measurements from these two sources to jointly estimate a vehicle’s speed and the scale factor of the wheel speed sensors. In addition, we analyze the performance of the estimators by use of the Cramér-Rao bound, and discuss the estimation of model parameters describing measurement errors and vehicle dynamics. Last, simulations and real-world data are used to show that the proposed estimators yield a substantial performance gain compared to when employing only one of the two measurement sources.

**Index Terms**—OBD, GNSS, insurance telematics, fleet management, driver behavior profiling.

## I. INTRODUCTION

Driver behavior profiling has received considerable attention in the literature, and is at the heart of many of today’s insurance telematics and fleet management programs [1], [2]. These programs have continuously gained in popularity over the last years, with the smart transportation market predicted to be worth around \$220 billion by 2021 [3]. Although there are many examples of trials or research studies using expensive, complex, or logistically demanding sensor setups [4], most of the major industry players (such as Progressive insurance, Allstate, Metromile, etc.) still primarily rely on speed measurements from the on-board diagnostics (OBD) system, and position and speed measurements from low-cost global navigation satellite system (GNSS) receivers [5], [6]. These implementations tend to be scalable, easy to deploy, and easy to understand for the users. An illustration of OBD and GNSS measurements of speed is provided in Fig. 1.

Some telematics providers have chosen to extract driving information also from inertial sensors [7]. On the one hand, incorporating inertial sensors into the sensor setup enables estimation of the vehicle’s orientation and direct estimation (not requiring differentiation) of the vehicle’s acceleration (which can be used to e.g., detect harsh braking events). In addition, inertial sensors tend to increase the estimation rate since commonly used inertial sensors can have sampling rates in the order of 100 [Hz] [8], while GNSS receivers used in telematics applications typically have an update rate of only

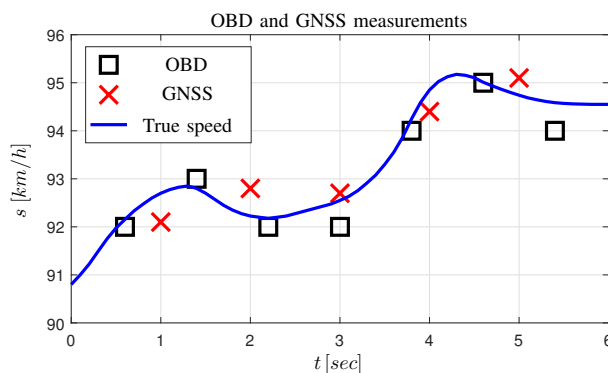


Fig. 1. Illustration of OBD and GNSS measurements of speed  $s$  as dependent on time  $t$ . Note that all OBD measurements are quantized as multiples of 1 [km/h].

1 [Hz]. On the other hand, making use of inertial sensors can be challenging for several reasons. When integrating inertial measurements to estimate for example the vehicle’s orientation, velocity, or position, errors will accumulate due to biases and random noise [9]. Moreover, in insurance telematics programs where inertial measurements are collected from smartphone-embedded sensors [10], problems often arise due to the fact that the smartphone is mobile with respect to the vehicle [11], [12]. The high sampling rate also tends to put strain on computational resources. Due to the aforementioned difficulties and the fact that most of the industry still primarily relies on OBD and GNSS measurements, this study will exclusively focus on the scenario where inertial sensors are absent. Furthermore, we note that fusion of measurements from inertial sensors and GNSS receivers is a mature technology that has been well-studied in the literature [13].

In this article, we employ OBD and GNSS measurements of speed to construct estimators of a vehicle’s speed and of the scale factor of the wheel speed sensors. Specifically, we demonstrate how to capitalize on the complementary characteristics of the OBD (bounded error when the scale factor is known) and GNSS (unbiased errors) measurements. Compared to when using either of these two sensors individually, the proposed sensor fusion method offers both a higher estimation rate and an enhanced estimation accuracy. In addition, speed estimates only based on OBD measurements will become more accurate once an accurate estimate of the scale factor is available. Hence, this implies an increased resilience to GNSS outages or other situations where GNSS measurements are not available (such as when one relies on GNSS measurements from a smartphone that during some drives may be discharged or not located in the car). The proposed method is appropriate for several sensor setups that are commonly used in current insurance telematics and fleet management programs. These setups include OBD dongles with an embedded GNSS tracker,

J. Wahlström is with the Dept. of Computer Science, University of Oxford (e-mail: [johan.wahlstrom@cs.ox.ac.uk](mailto:johan.wahlstrom@cs.ox.ac.uk)).

R. Larsson Nordström and P. Händel are with the ACCESS Linnaeus Center, Dept. of Information Science and Engineering, KTH Royal Institute of Technology, Stockholm, Sweden (e-mail: {robinl, ph}@kth.se).

I. Skog is with the Dept. of Electrical Engineering, Linköping University, Sweden (e-mail: [isaac.skog@liu.se](mailto:isaac.skog@liu.se)).

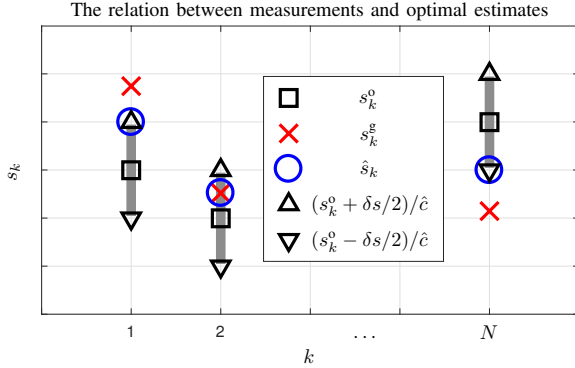


Fig. 2. Illustration of the relation between measurements and ML estimates under the assumption of synchronous measurements.

and OBD dongles connected to GNSS-equipped smartphones. The speed estimates resulting from the proposed sensor fusion could e.g., be differentiated to construct acceleration estimates for the detection of harsh braking or acceleration, be used to detect speeding, or be used as input in traffic flow models. While insurance telematics and fleet management are our main motivations, the mentioned capabilities could also be of use in e.g., urban planning and general traffic surveillance, where the aim might be to reduce congestion or detect anomalous traffic patterns. Additionally, the speed estimates could be used within accident reconstruction [14], or for detecting the use of cruise control.

Since the scale factor is slowly time-varying, we also describe how to test for changes in the scale factor. This could be used to assess overall tire pressure and detect flat tires. By maintaining recommended tire inflation pressure, it is possible to not only improve fuel economy and handling, but also to reduce tire wear, noise emissions, braking distances, and rolling resistance. Proper tire inflation has been estimated to reduce carbon dioxide emissions by about 2.5% [15]. As opposed to standard indirect tire-pressure monitoring systems (TPMSs), the tire-pressure monitor presented here can be used to detect underinflation also when the four tires are equally underinflated [16].

## II. ESTIMATION

This section presents maximum likelihood (ML) and maximum a posteriori (MAP) estimators for the problem of using OBD and GNSS measurements of speed to jointly estimate a vehicle's speed and the scale factor of the OBD wheel speed sensors. We begin by considering the case when the OBD and GNSS samples can be assumed to be time synchronized, and then examine the same problem but with asynchronous samples. While the latter model is more realistic, the former enables both a simpler estimation algorithm and more straightforward Cramér-Rao studies in Section III.

### A. Synchronous Samples

For the case with synchronous samples, there exists both OBD and GNSS measurements at every sampling instance  $k$

where measurements are taken. The measurements obtained at sampling instance  $k$  are modeled according to<sup>1</sup>

$$s_k^o = cs_k + q_k, \quad (1a)$$

$$s_k^g = s_k + \epsilon_k. \quad (1b)$$

Here,  $s^o$  and  $s^g$  denote measurements of speed obtained from the OBD system and GNSS receiver, respectively. Further,  $s$  is the speed of the vehicle,  $c$  is an unknown positive scale factor arising due to the uncertainty of the wheel radius<sup>2</sup> [19],  $q$  is the quantization error of the OBD system, and  $e$  is the measurement error of the GNSS receiver. The quantization is made so that  $s_k^o = n \cdot \delta s$  for some nonnegative integer  $n$  and some positive quantization interval  $\delta s$ , with  $q_k \in [-\delta s/2, \delta s/2]$ . In practice, we have  $n = 0, 1, \dots, 255$  and  $\delta s = 1 [km/h]$  [20]. Although there are other errors present in OBD measurements of speed [21] (such as wheel slips, discussed in Section II-E), the scale factor and quantization errors are typically dominant. The GNSS measurement error  $e_k$  is assumed to be normally distributed and white with variance  $\sigma_g^2$  (normally distributed errors is a common assumption for GNSS position measurements along a single spatial dimension [22]).

Let us assume that we have made the measurements  $\mathbf{s}^o \triangleq [s_1^o \dots s_N^o]^\top$  and  $\mathbf{s}^g \triangleq [s_1^g \dots s_N^g]^\top$  from the OBD system and the GNSS receiver, respectively. The ML estimates of the speeds  $\mathbf{s} \triangleq [s_1 \dots s_N]^\top$  and the scale factor  $c$  are then given by

$$\{\hat{\mathbf{s}}, \hat{c}\} = \arg \max_{\mathbf{s}, c} p(\mathbf{s}^o, \mathbf{s}^g | \mathbf{s}, c) \quad (2)$$

where  $p(\cdot | \cdot)$  denotes a conditional probability density function. The likelihood function can be factorized as

$$\begin{aligned} p(\mathbf{s}^o, \mathbf{s}^g | \mathbf{s}, c) &= p(\mathbf{s}^o | \mathbf{s}, c) p(\mathbf{s}^g | \mathbf{s}) \\ &= \prod_{k=1}^N p(s_k^o | s_k, c) p(s_k^g | s_k). \end{aligned} \quad (3)$$

Now, noting that  $p(s_k^g | s_k)$  is normally distributed with mean  $s_k$  and variance  $\sigma_g^2$ , while  $p(s_k^o | s_k, c) \propto \mathbf{1}\{|cs_k - s_k^o| \leq \delta s/2\}$ <sup>3</sup>, where  $\mathbf{1}\{\cdot\}$  denotes the indicator function, it follows that the ML estimates in (2) can be found as the solution to the constrained nonlinear optimization problem

$$\begin{aligned} &\underset{\mathbf{s}, c}{\text{minimize}} \quad \sum_{k=1}^N (s_k - s_k^g)^2 \\ &\text{subject to} \quad |cs_k - s_k^o| \leq \delta s/2 \text{ for } k = 1, \dots, N. \end{aligned} \quad (4)$$

<sup>1</sup>It should be noted that the presented model does not explicitly consider GNSS position measurements. Generally, speed estimates derived from GNSS position measurements are not sufficiently accurate to be used to improve upon doppler-based GNSS measurements of speed [17]. As a result, it is sensible to exclude GNSS position measurements from model (1).

<sup>2</sup>Although it is typically possible to extract speed measurements from each of the wheels individually by using the controller area network (CAN) bus [18], most off-the-shelf telematics devices will extract a scalar speed measurement from the standardized OBD-II parameter IDs (PIDs). Hence, the scale factor  $c$  is the "average" scale factor among the wheels that were used to construct the measurement  $s^o$ .

<sup>3</sup>Although assuming e.g.,  $q_k \in (-\delta s/2, \delta s/2]$  and  $p(s_k^o | s_k, c) \propto \mathbf{1}\{-\delta s/2 \leq cs_k - s_k^o < \delta s/2\}$  would make the quantization function deterministic and be somewhat more stringent, we choose, for notational reasons, to include both boundaries in the permissible parameter set. For all practical purposes, this will not alter the considered estimation problem. Further, for notational simplicity, we disregard the case when  $s_k^o = 0$ , which gives  $p(s_k^o | s_k, c) \propto \mathbf{1}\{0 \leq cs_k - s_k^o \leq \delta s/2\}$ .

Although (4) is nonconvex, it can be parameterized as the equivalent one-dimensional unconstrained convex optimization problem

$$\underset{d}{\text{minimize}} \sum_{k=1}^N (f_k(d) - s_k^g)^2 \quad (5)$$

where

$$f_k(d) \triangleq \begin{cases} s_k^g, & |s_k^g/d - s_k^o| \leq \delta s/2 \\ (s_k^o + \delta s/2)d, & s_k^g/d - s_k^o > \delta s/2 \\ (s_k^o - \delta s/2)d, & s_k^g/d - s_k^o < -\delta s/2. \end{cases} \quad (6)$$

The problem (5) is readily solved using e.g., Newton's method, and the optimal parameters to (4) can then be found as  $\hat{s}_k = f_k(\hat{d})$  and  $\hat{c} = 1/\hat{d}$ , where  $\hat{d}$  is the optimal solution to (5). If there is no  $d$  such that  $|s_k^g/d - s_k^o| \leq \delta s/2$  for  $k = 1, \dots, N$ , the optimization function in (5) is strictly convex and the ML estimates are unique. The solution to the optimization problem described by (5) and (6) is visualized in Fig. 2. It is easy to verify that the equivalent optimization problem parameterized with the optimization variable  $c = 1/d$  is *not* guaranteed to be convex.

### B. Asynchronous Samples

In general, the OBD and GNSS measurements cannot be assumed to be synchronous. Taking this into account, the measurement model in (1) is modified according to

$$s_k^o = cs_k + q_k, \quad k \in \mathcal{O}, \quad (7a)$$

$$s_k^g = s_k + \epsilon_k, \quad k \in \mathcal{G}. \quad (7b)$$

Here,  $\mathcal{O}$  and  $\mathcal{G}$  denote the sampling instances where there are OBD and GNSS measurements, respectively. It is assumed that  $\mathcal{O} \cup \mathcal{G} = \{1, \dots, N\}$ . Further, the measurement errors are assumed to have the same distributions as in (1).

Now, let us follow the approach of the previous subsection to find ML estimates of  $\mathbf{s} \triangleq [s_1 \dots s_N]^\top$  and  $c$  from (7). The ML estimates of  $\{s_k : k \in \mathcal{O} \cap \mathcal{G}\}$  and  $c$  are obtained by applying the method presented for synchronous samples. Obviously, the resulting optimization problem need only consider measurements made at sampling instances in  $\mathcal{O} \cap \mathcal{G}$ . If  $\mathcal{O} \cap \mathcal{G} = \emptyset$ , it is not possible to estimate  $c$ . Since the ML estimate of  $s_k$  for  $k \in \mathcal{O} \cap \mathcal{G}$  (i.e., at sampling instances where only OBD measurements are available) is obtained as  $\hat{s}_k = \arg \max_{s_k} p(s_k^o | s_k, \hat{c}) = \arg \max_{s_k} \mathbf{1}\{|\hat{c}s_k - s_k^o| \leq \delta s/2\}$ , there is no ML estimate of  $s_k$  for  $k \in \mathcal{O} \cap \bar{\mathcal{G}}$  unless there is an ML estimate of  $c$ . Moreover, even if there exists an ML estimate of  $c$ , there is no unique ML estimate of  $s_k$  for  $k \in \mathcal{O} \cap \bar{\mathcal{G}}$ . Here,  $\bar{\mathcal{A}}$  denotes the complement of a set  $\mathcal{A}$ . Further, we note that  $\hat{s}_k = \arg \max_{s_k} p(s_k^g | s_k) = s_k^g$  for any  $k \in \bar{\mathcal{O}} \cap \mathcal{G}$ . To summarize, by relaxing the assumption of synchronous measurements, the following issues arise: 1) if there are no sampling instances with concurrent OBD and GNSS measurements neither the scale factor, nor the speed at sampling instances where only OBD measurements are available, can be estimated by means of ML; 2) there is no unique ML estimate of the speed at sampling instances where only OBD measurements are available; and 3) at sampling

instances where only GNSS measurements are available the ML estimates are no better than the GNSS measurements.

One way to resolve these issues is to introduce a dynamic model for the vehicle speeds. Here, we use the model

$$s_{k+1} = s_k + w_k \quad (8)$$

where  $w_k$  is assumed to be normally distributed and white with variance  $\Delta t_k \sigma_s^2$ , and  $\Delta t_k$  denotes the sampling interval between sampling instances  $k$  and  $k+1$ . By incorporating this dynamic model as a prior  $p(\mathbf{s})$  on the vehicle speeds, the MAP estimates of  $\mathbf{s}$  and  $c$  are obtained as

$$\{\hat{\mathbf{s}}, \hat{c}\} = \arg \max_{\mathbf{s}, c} p(\mathbf{s}, c | \mathbf{s}^o, \mathbf{s}^g) \quad (9)$$

where  $\mathbf{s}^o \triangleq \{s_k^o\}_{k \in \mathcal{O}}$  and  $\mathbf{s}^g \triangleq \{s_k^g\}_{k \in \mathcal{G}}$ . The posterior can be factorized as

$$\begin{aligned} p(\mathbf{s}, c | \mathbf{s}^o, \mathbf{s}^g) &\propto p(\mathbf{s}^o, \mathbf{s}^g | \mathbf{s}, c) p(\mathbf{s}, c) \\ &= p(\mathbf{s}^o | \mathbf{s}, c) p(\mathbf{s}^g | \mathbf{s}) p(\mathbf{s}) \\ &= \prod_{k \in \mathcal{O}} p(s_k^o | s_k, c) \prod_{k \in \mathcal{G}} p(s_k^g | s_k) \\ &\quad \cdot \prod_{k=1}^{N-1} p(s_{k+1} | s_k) \end{aligned} \quad (10)$$

where we have used the uninformative priors  $p(c) \propto 1$  and  $p(s_1) \propto 1$  on the scale factor and the initial speed, respectively. It now follows that the MAP estimates can be found as the solution to the constrained nonlinear optimization problem

$$\begin{aligned} \underset{\mathbf{s}, c}{\text{minimize}} \quad & \frac{1}{\sigma_g^2} \sum_{k \in \mathcal{G}} (s_k - s_k^g)^2 + \frac{1}{\sigma_s^2} \sum_{k=1}^{N-1} \frac{1}{\Delta t_k} (s_{k+1} - s_k)^2 \\ \text{subject to} \quad & |cs_k - s_k^o| \leq \delta s/2 \text{ for } k \in \mathcal{O}, \end{aligned} \quad (11)$$

which can be solved using e.g., interior-point methods [23].

### C. Estimation of Model Parameters

To solve the optimization problem (11), we need the two model parameters  $\sigma_g^2$  and  $\sigma_s^2$ . While (11) can be seen to only depend on the ratio  $\sigma_g^2/\sigma_s^2$ , identifying the parameters  $\sigma_g^2$  and  $\sigma_s^2$  will be easier if we estimate the two parameters separately. Hence, when  $\sigma_g^2$  and  $\sigma_s^2$  are considered to be unknown, we will make use of the expectation maximization (EM) algorithm with  $\boldsymbol{\theta} \triangleq [\sigma_g^2 \ \sigma_s^2]^\top$  as the parameter vector to be estimated,  $\{\mathbf{s}, c\}$  as the missing data, and  $\{\mathbf{s}^g, \mathbf{s}^o\}$  as the observed data. Consequently,  $\boldsymbol{\theta}$  is iteratively estimated according to

$$\hat{\sigma}_{g,i+1}^2 = \frac{1}{|\mathcal{G}|} \sum_{k \in \mathcal{G}} \mathbb{E}_{p_{\boldsymbol{\theta}^{(i)}}(s_k | \mathbf{s}^o, \mathbf{s}^g)} [(s_k - s_k^g)^2], \quad (12a)$$

$$\hat{\sigma}_{s,i+1}^2 = \frac{1}{N-1} \sum_{k=1}^{N-1} \frac{1}{\Delta t_k} \mathbb{E}_{p_{\boldsymbol{\theta}^{(i)}}(s_k, s_{k+1} | \mathbf{s}^o, \mathbf{s}^g)} [(s_{k+1} - s_k)^2], \quad (12b)$$

where  $\boldsymbol{\theta}^{(i)} \triangleq [\hat{\sigma}_{g,i}^2 \ \hat{\sigma}_{s,i}^2]^\top$  and  $\mathbb{E}_p[\cdot]$  is the expectation with respect to the probability density function  $p$ . A derivation of (12) is given in Appendix A. Since we do not know  $p_{\boldsymbol{\theta}^{(i)}}(s_k | \mathbf{s}^o, \mathbf{s}^g)$  or  $p_{\boldsymbol{\theta}^{(i)}}(s_k, s_{k+1} | \mathbf{s}^o, \mathbf{s}^g)$ , we will use the stan-

standard approximation [24]

$$\mathbb{E}_{p_{\theta^{(i)}}(s_k | s^o, s^g)} [(s_k - s_k^g)^2] \approx (\hat{s}_k - s_k^g)^2, \quad (13a)$$

$$\mathbb{E}_{p_{\theta^{(i)}}(s_k, s_{k+1} | s^o, s^g)} [(s_{k+1} - s_k)^2] \approx (\hat{s}_{k+1} - \hat{s}_k)^2, \quad (13b)$$

where  $\hat{s}_k$  is the MAP estimate of  $s_k$  given  $\theta^{(i)}$ .

#### D. Testing for Changes in the Scale Factor

For the purpose of developing a TPMS, let us consider the setting with synchronous samples described in Section II-A. The speeds  $\mathbf{s} \triangleq \{\mathbf{s}^{(1)}, \mathbf{s}^{(2)}\}$  are measured as  $\mathbf{s}^o \triangleq \{\mathbf{s}^{o1}, \mathbf{s}^{o2}\}$  and  $\mathbf{s}^g \triangleq \{\mathbf{s}^{g1}, \mathbf{s}^{g2}\}$ , where  $\mathbf{s}^{(1)} \triangleq \{s_k\}_{k \in \mathcal{S}^{(1)}}$ ,  $\mathbf{s}^{(2)} \triangleq \{s_k\}_{k \in \mathcal{S}^{(2)}}$ ,  $\mathbf{s}^{o1} \triangleq \{s_k^o\}_{k \in \mathcal{S}^{(1)}}$ ,  $\mathbf{s}^{o2} \triangleq \{s_k^o\}_{k \in \mathcal{S}^{(2)}}$ ,  $\mathbf{s}^{g1} \triangleq \{s_k^g\}_{k \in \mathcal{S}^{(1)}}$ , and  $\mathbf{s}^{g2} \triangleq \{s_k^g\}_{k \in \mathcal{S}^{(2)}}$ , while  $\mathcal{S}^{(1)} = \{1, \dots, N_1\}$  and  $\mathcal{S}^{(2)} = \{N_1 + 1, \dots, N\}$ . To test whether the scale factor is different in  $\mathbf{s}^{o1}$  and  $\mathbf{s}^{o2}$ , let us formulate the null hypothesis

$$\mathcal{H}_0 : c^{(1)} = c^{(2)} \quad (14)$$

where  $c^{(1)}$  and  $c^{(2)}$  denote the scale factors in  $\mathbf{s}^{o1}$  and  $\mathbf{s}^{o2}$ , respectively. The null hypothesis is conveniently tested by computing the generalized likelihood ratio (GLR) [25]

$$\Lambda(\mathbf{s}^o, \mathbf{s}^g) = \frac{\arg \max_{\mathbf{s}, c^{(1)}=c^{(2)}} p(\mathbf{s}^o, \mathbf{s}^g | \mathbf{s}, c^{(1)}, c^{(2)})}{\arg \max_{\mathbf{s}, c^{(1)}, c^{(2)}} p(\mathbf{s}^o, \mathbf{s}^g | \mathbf{s}, c^{(1)}, c^{(2)})} \quad (15)$$

and deciding on  $\mathcal{H}_0$  whenever  $\Lambda(\mathbf{s}^o, \mathbf{s}^g) > \eta$  for some chosen threshold  $\eta$ . The optimal parameters in the numerator are the ML estimates of  $\mathbf{s}$  and  $c^{(1)} = c^{(2)}$  obtained from  $\mathbf{s}^o$  and  $\mathbf{s}^g$ , while the optimal parameters in the denominator are the ML estimates of  $\mathbf{s}^{(1)}$  and  $c^{(1)}$  obtained from  $\mathbf{s}^{o1}$  and  $\mathbf{s}^{g1}$ , and the ML estimates of  $\mathbf{s}^{(2)}$  and  $c^{(2)}$  obtained from  $\mathbf{s}^{o2}$  and  $\mathbf{s}^{g2}$ . The generalization to the case with asynchronous samples is straightforward.

#### E. Additional Error Sources

We will now briefly discuss two error sources that have been disregarded in the measurement models (1) and (7). Firstly, during wheel slips, the speed of the vehicle differs from the tangential speed of the wheels. As a result, the OBD measurements will be distorted. The effect is typically small during smooth driving on a dry surface. However, if the wheel slips need to be compensated for, one may use that there is an approximately linear relation between the vehicle's acceleration and the ratio of the tangential wheel speed and the longitudinal speed of the vehicle [26]. Secondly, most low-cost GNSS receivers only provide speed measurements in the two-dimensional plane that is tangential to the surface of the earth. Consequently, the speed measurements obtained from a GNSS receiver will tend to be lower than the true three-dimensional speed when travelling along steep inclines. This effect may be compensated for by using data from a three-dimensional road map.

### III. THE CRAMÉR-RAO BOUND

The Cramér-Rao bound (CRB) will now be used to gain some insight into the estimation problems discussed in the

preceding section. For brevity and tractability, the analysis will be focused on the case with synchronous samples investigated in Section II-A. The CRB can be formulated as [27]

$$\text{Cov}(\hat{\mathbf{x}}) \succeq \mathbf{P} \quad (16)$$

and holds for any unbiased estimator  $\hat{\mathbf{x}}$  of  $\mathbf{x} \triangleq [\mathbf{s}^\top \ c]^\top$ . Here,  $\mathbf{P}$  is the inverse of the Fisher information matrix (FIM), and we have used  $\mathbf{A} \succeq \mathbf{B}$  to denote that  $\mathbf{A} - \mathbf{B}$  is positive semidefinite. The FIM is defined as  $\mathcal{I} \triangleq \mathbb{E}_{p(\mathbf{s}^o, \mathbf{s}^g | \mathbf{x})} [(\partial_{\mathbf{x}} \ln p(\mathbf{s}^o, \mathbf{s}^g | \mathbf{x}))^\top \partial_{\mathbf{x}} \ln p(\mathbf{s}^o, \mathbf{s}^g | \mathbf{x})]$ , where  $(\partial_{\mathbf{x}} \ln p(\mathbf{s}^o, \mathbf{s}^g | \mathbf{x}))^\top$  is the gradient of the log-likelihood function (the score function) with respect to  $\mathbf{x}$ .

As evident from the optimization problem (4), the information gained from the OBD measurements can be transformed into inequality constraints on the ML estimates. Since imposing inequality constraints on parameter estimates do not alter the FIM [28], it follows that to compute the FIM, one only needs to consider the GNSS measurements. The resulting FIM is singular (no Fisher information is gained about the scale factor) and not very interesting since it merely allows us to recover the accuracy of the GNSS measurements, which we obviously can expect to surpass when also OBD measurements are available. One way to obtain more useful results is by instead studying the CRB of a closely related problem. This approach will be considered next.

#### A. Bounds under Equality Constraints

Let us assume that some of the inequality constraints originating from the OBD measurements can be transformed into equality constraints. Thus, we consider the problem of estimating  $\mathbf{s}$  and  $c$  from  $p(\mathbf{s}^o, \mathbf{s}^g | \mathbf{s}, c)$  under the constraints  $cs_k - s_k^o = \gamma_k$  for  $k = M + 1, \dots, N$ . Here,  $\gamma_k \in [-\delta s/2, \delta s/2]$  is a constant and  $M$  is the number of samples for which there are no associated equality constraints<sup>4</sup>. It is assumed that  $M < N$ , i.e., that at least one equality constraint exists. Since we are adding information to the original problem, the CRB for this new problem will still be a lower bound for the original problem. As shown in Appendix B, the inverse FIM for our new constrained estimation problem takes the form

$$\mathbf{P} = \sigma_g^2 \begin{bmatrix} \mathbf{I}_M & \mathbf{0}_{M, N-M+1} \\ \mathbf{0}_{N-M+1, M} & \boldsymbol{\varphi} \boldsymbol{\varphi}^\top / \alpha \end{bmatrix} \quad (17)$$

where  $\boldsymbol{\varphi} \triangleq [\mathbf{s}_{M+1:N}^\top - c]^\top$ ,  $\mathbf{s}_{M+1:N} \triangleq [s_{M+1} \ \dots \ s_N]^\top$ , and  $\alpha \triangleq \sum_{k=M+1}^N s_k^2$ . Moreover,  $\mathbf{I}_\ell$  and  $\mathbf{0}_{\ell_1, \ell_2}$  denote the identity and zero matrices of dimensions  $\ell$  and  $\ell_1 \times \ell_2$ , respectively. Studying the diagonal elements of  $\mathbf{P}$  we obtain the scalar CRBs

$$\text{Var}(\hat{s}_k) \geq \sigma_g^2 \quad (18a)$$

<sup>4</sup>It is important to note that the order of the speed measurements in Section II-A is ambiguous. Hence, assuming that we add the equality constraints  $cs_k - s_k^o = \gamma_k$  to  $N - M$  randomly chosen sampling instances, it is always possible to redefine the indices of the measurements so that only the last  $N - M$  speed measurements are subject to equality constraints.

for  $k = 1, \dots, M$ ,

$$\text{Var}(\hat{s}_k) \geq \sigma_g^2 \frac{s_k^2}{\sum_{k=M+1}^N s_k^2} \quad (18b)$$

for  $k = M + 1, \dots, N$ , and

$$\text{Var}(\hat{c}) \geq \sigma_g^2 \frac{c^2}{\sum_{k=M+1}^N s_k^2}. \quad (18c)$$

Assuming that the CRBs give an indication of the performance of the estimator derived in Section II-A, this means that estimates of  $s_{M+1}, \dots, s_N$ , and  $c$  tend to improve as the number of equality constraints increases ( $M$  becomes smaller). Relating back to the original problem in Section II-A, an increasing number equality constraints should be interpreted as smaller  $\delta s$  since this means that the inequality constraints become tighter (obviously,  $\delta s = 0$  implies that  $|cs_k - s_k^o| \leq \delta s/2$  is the equality constraint  $cs_k - s_k^o = \gamma_k$  with  $\gamma_k = 0$ ). Similarly, estimates of  $c$  tend to improve at higher speeds and with smaller scale factors. Naturally, all estimates can be expected to improve as the noise variance of the GNSS measurements decrease. The qualitative conclusions drawn from the CRB studies are validated by means of numerical simulations in Section IV-A.

### B. Comments on the Equality Constraints

We will now further illuminate the relation between the estimation problem considered in Section II-A and the estimation problem with equality constraints considered in Section III-A. To begin with, consider the same estimation problem as in Section II-A but with an added prior  $p(c) \propto \mathbf{1}\{c^{\text{low}} \leq c \leq c^{\text{high}}\}$  on the scale factor. Then, assuming no prior information on the speeds  $s$ , the MAP estimates of  $s$  and  $c$  can be computed from the optimization problem in (4) but with the added constraint  $c^{\text{low}} \leq c \leq c^{\text{high}}$ . Similarly, one may use the optimization problem in (5) but with the added constraint  $1/c^{\text{high}} \leq d \leq 1/c^{\text{low}}$ . Since  $\hat{s}_k \in [(s_k^o - \delta s/2)/c^{\text{high}}, (s_k^o + \delta s/2)/c^{\text{low}}]$ , it can easily be seen that if  $c^{\text{low}} s_k^g - s_k^o > \delta s/2$  for some  $k$ , we can replace the inequality constraint  $|cs_k - s_k^o| \leq \delta s/2$  with the equality constraint  $cs_k - s_k^o = \delta s/2$ . Likewise, if  $c^{\text{high}} s_k^g - s_k^o < -\delta s/2$  for some  $k$ , we can replace the inequality constraint  $|cs_k - s_k^o| \leq \delta s/2$  with the equality constraint  $cs_k - s_k^o = -\delta s/2$ . To summarize, some of the inequality constraints in the optimization problem (4) might, under the assumption that we add constraints (a rectangular prior) on the scale factor, be replaced by equality constraints of the same type that was considered in Section III-A. However, which (if any) constraints that can be reformulated in this way will be dependent on the obtained measurements, and hence, this is *not* a general reformulation of the estimation problem (4) with an added prior on the scale factor.

## IV. EXPERIMENTAL STUDY

To evaluate the estimators, data from inertial sensors and GNSS receivers were recorded from cars in two different scenarios: The first data set captured high-speed driving on a race track and was recorded using a car-mounted Samsung Galaxy S III. The second data set reflected driving at modest speeds in a suburban environment and was recorded using a

TABLE I  
STUDIED DATA SETS.

Data set	1	2
Environment	Race track	Suburban
Top speed [km/h]	181.9	42.5
Average speed [km/h]	94.6	33.3

Microstrain 3DM-GX3-35 positioned on the roof of the car. Both data sets consists of about two minutes of data. Summary statistics of the data sets are provided in Table I.

The data was fused in a GNSS-aided inertial navigation system (INS) [19], and speed estimates were extracted by taking the norm of the three-dimensional velocity estimates. Hence, both data sets produced two minutes of speed estimates at 20 [Hz] (the same update rate as the inertial sensors). Next, we will investigate the performance of the estimators presented in Section II by simulating measurements from these speed sequences, which will be treated as ground truth  $s$ . In other words, the ground truth can be considered to be “perfect” in the sense that the true measurement errors of the collected real-world data should not be expected to have any impact on the estimation accuracies resulting from the field study. Since the measurement errors are simulated, they will not be affected by wheel slips or steep road inclines (see Section II-E).

Unless otherwise stated, we will simulate the scale factor  $c$  from  $\mathcal{U}(\bar{c} - 0.02, \bar{c} + 0.02)$  with  $\bar{c} = 1$ , where  $\mathcal{U}(a, b)$  denotes the uniform distribution over the interval  $(a, b)$ <sup>5</sup>. Similarly, we will use the default values  $\delta s = 1$  [km/h] and  $\sigma_g = 0.2 \cdot 3.6$  [km/h] [29]. We wish to emphasize that no real-world OBD measurements were recorded. Rather, OBD and GNSS measurements were simulated from a ground truth speed sequence that was obtained by fusing real-world GNSS and inertial measurements. Hence, the simulated OBD and GNSS measurements did not need to be time-synchronized.

### A. Experimental Study — Synchronous Samples

Synchronous OBD and GNSS measurements were simulated with a sampling rate of 1 [Hz]. Fig. 3 displays root-mean-square errors (RMSEs) of the scale factor estimates obtained from the ML estimator presented in Section II-A. Each marker in the plots was obtained as the result of  $10^5$  simulations. As can easily be seen, Fig. 3 confirms the qualitative conclusions drawn from the CRB studies in Section III-A. Specifically, the estimates improve at higher speeds, at higher OBD resolutions (lower  $\delta s$ ), at lower GNSS error variances, and at lower scale factors. Moreover, as suggested by the CRB in (18c), the RMSE can be seen to grow approximately linearly with  $\sigma_g$  and  $c$ . Note that the CRB presented in Section III-A is not the CRB for the model in Section II-A (as concluded in Section III, the FIM for this estimation problem is singular). Hence, there is no quantitative comparison to be made between the RMSEs and the derived CRB.

<sup>5</sup>Scale factor errors in the order of 1 percent can occur due to changes in pressure, temperature, and load, while tire wear can reduce the scale factor by up to 3 percent [19].

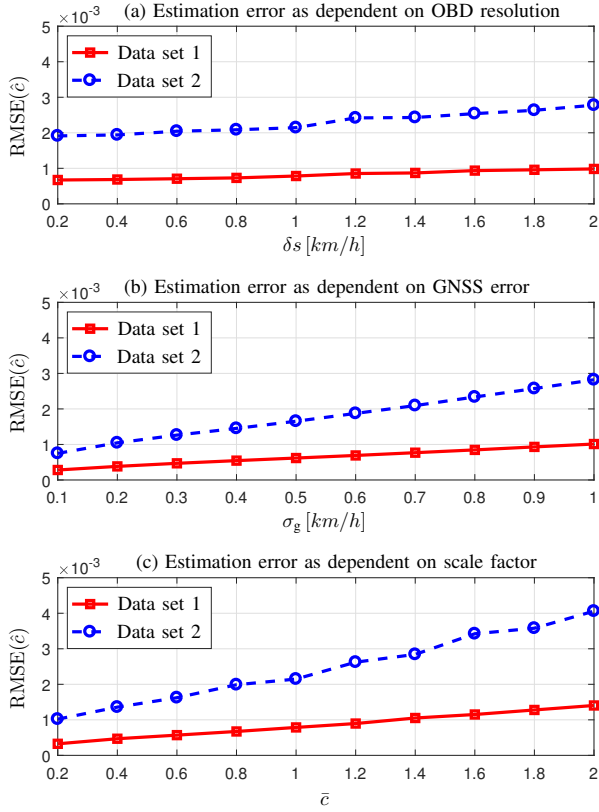


Fig. 3. Errors of scale factor estimates based on synchronous measurements.

As indicated by the CRB in (18b), Fig. 4 (a) shows that the speed estimates improve as the OBD resolution increases, and that their accuracy is independent of the magnitude of the speeds. In Figs. 4 (b) and (c), the ML estimator is compared to the estimators  $\hat{s} = s^o$  and  $\hat{s} = s^g$ , from hereon referred to as the OBD estimator and GNSS estimator, respectively. Obviously, the accuracy of the OBD estimator is independent of  $\sigma_g$ , while the RMSE of the GNSS estimator is exactly equal to  $\sigma_g$ . The RMSE of the OBD estimator is larger on the first data set since this has higher speeds and thereby produces larger scale factor errors. The ML estimator improves upon the accuracy of the individual measurement sources in both cases. For small GNSS error variances, the OBD measurements do not add much information to the GNSS measurements and the RMSE of the ML estimator can be seen to approach  $\sigma_g$ .

### B. Experimental Study — Asynchronous Samples

Asynchronous OBD and GNSS measurements were simulated with sampling intervals of 0.9 [s] and 1 [s], respectively, with the first OBD and GNSS measurements assumed to be synchronous<sup>6</sup>. Each marker in the plots was obtained as the result of  $10^4$  simulations. We will begin by comparing the MAP estimator presented in Section II-B to the OBD and GNSS estimators (which only estimate the speed at the sampling instances with OBD and GNSS measurements, respectively). To achieve a fair comparison, the prior  $p(s)$

<sup>6</sup>Mathematically, the OBD and GNSS signals were sampled at the time points  $t_k^o = k \cdot \Delta t^o$  and  $t_k^g = k \cdot \Delta t^g + t_c$ , respectively. Here,  $\Delta t^o = 0.9$  [s] and  $\Delta t^g = 1$  [s], while  $t_c$  was chosen so that  $t_1^o = t_1^g$ .

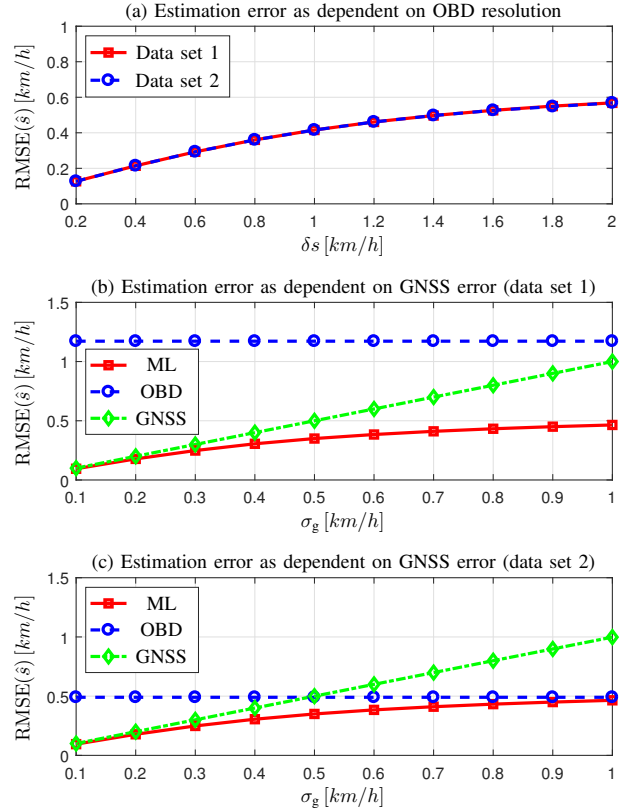


Fig. 4. Errors of speed estimates based on synchronous measurements.

was added to the GNSS estimator. In other words, the GNSS estimator was defined as  $\hat{s} = \arg \max_s p(s^g | s) p(s)$ , while the OBD estimator was defined as  $\hat{s} = s^o$ . Attempts to incorporate the prior  $p(s)$  into the OBD estimator by defining it according to  $\hat{s} = \arg \max_s p(s^o | s, c = 1) p(s)$  did not result in any performance gain. For clarity, the RMSE of the MAP estimator has been divided into two parts. These are denoted MAP<sup>o</sup> and MAP<sup>g</sup>, and only account for the errors at sampling instances with OBD and GNSS measurements, respectively.

Fig. 5 displays the RMSEs when using  $\sigma_s = 1.5$  [ $m/s^2/\sqrt{Hz}$ ] and  $\sigma_s = 0.25$  [ $m/s^2/\sqrt{Hz}$ ] on the first and second data set, respectively. These values of  $\sigma_s$  are roughly equal to the dynamic variation  $(1/(N-1) \cdot \sum_{k=1}^{N-1} (s_{k+1} - s_k)^2 / \Delta t_k)^{1/2}$  when  $\Delta t_k = 1$  [s]. In contrast, Fig. 6 shows the RMSEs that were obtained when  $\sigma_g$  and  $\sigma_s$  were estimated using the EM algorithm described in Section II-C. The EM recursions were terminated when  $\|\theta^{(i+1)} - \theta^{(i)}\| < 0.01$  or when 10 iterations had been completed. As can be seen in Figs. 5 and 6, the MAP estimator outperforms the OBD and GNSS estimators on both data sets; both when fixing the model parameters and when estimating them using the EM algorithm. In similarity with the results displayed for synchronous measurements in Figs. 4 (b) and (c), the RMSE of MAP<sup>g</sup> approaches that of the GNSS estimator for small  $\sigma_g$ . However, with asynchronous measurements, the MAP and GNSS estimators perform better on the second data set than on the first. This is a consequence of the second data set having lower dynamic variation. Thanks to the prior  $p(s)$ , the RMSE of the GNSS estimator is significantly lower than  $\sigma_g$  in Fig. 5 (b). However, in Fig. 6 (b), the added information from the

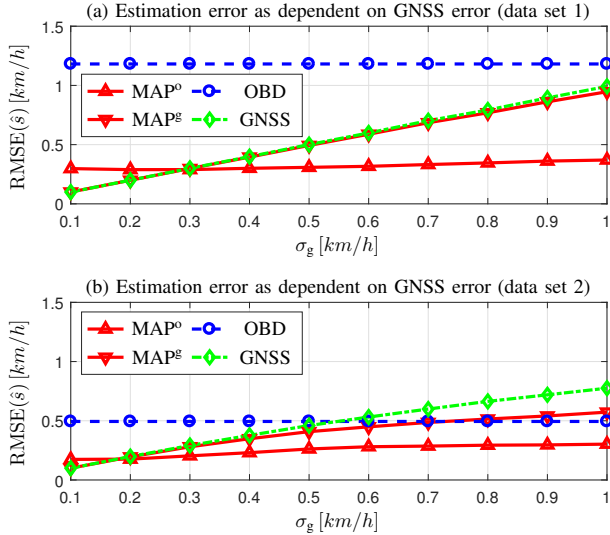


Fig. 5. Errors of speed estimates based on asynchronous measurements.

prior is offset by the uncertainty in the estimates of  $\sigma_g$  and  $\sigma_s$ , and the RMSE is once again in the vicinity of  $\sigma_g$ . As illustrated in Figs. 5 (a) and 6 (a), the RMSEs of MAP<sup>g</sup> and the GNSS estimator are roughly equal on the first data set. By comparison, MAP<sup>o</sup> outperforms the OBD measurements with a wide margin for all  $\sigma_g$ .

### C. Experimental Study — Hypothesis Testing

To illustrate the performance of the hypothesis testing described in Section II-D, synchronous measurements were simulated from both data sets as described in Section IV-A. In other words, the first and second data sets were associated with the sets  $\mathcal{S}^{(1)}$  and  $\mathcal{S}^{(2)}$ , respectively. The true positive rate was computed as follows. In each simulation, a scale factor  $c$  was generated for the first data set, while the second data set used the scale factor  $c + \delta c$ . For a given threshold, the true positive rate was defined as the percentage of simulations where the null hypothesis was rejected. To compute the false positive rate, the simulated scale factor  $c$  was used for both data sets. The false positive rate was then defined as the percentage of simulations where the null hypothesis was rejected. Fig. 7 displays the receiver operating characteristics (ROC) of the likelihood ratio for four different values of  $\delta c$ , with each true and false positive rate computed based on  $10^5$  simulations. The detector can be seen to reach excellent performance already at  $\delta c = 0.01$ .

## V. SUMMARY

This article addressed the problem of fusing OBD and GNSS measurements of speed to estimate a vehicle's speed and the scale factor of the OBD measurements. Under the assumption of synchronous samples, it was shown that the ML estimates can be extracted from the solution to a one-dimensional convex optimization problem. For the case with asynchronous samples, we analyzed the identifiability of the likelihood function and argued for the inclusion of a prior on the vehicle dynamics. Thus, the vehicle speed was modeled as a random walk with normally distributed steps, and the MAP

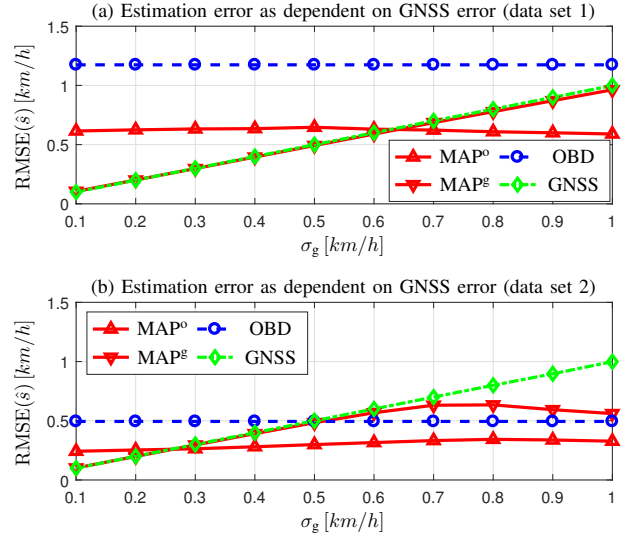


Fig. 6. Errors of speed estimates based on asynchronous measurements and when estimating the model parameters using the EM algorithm.

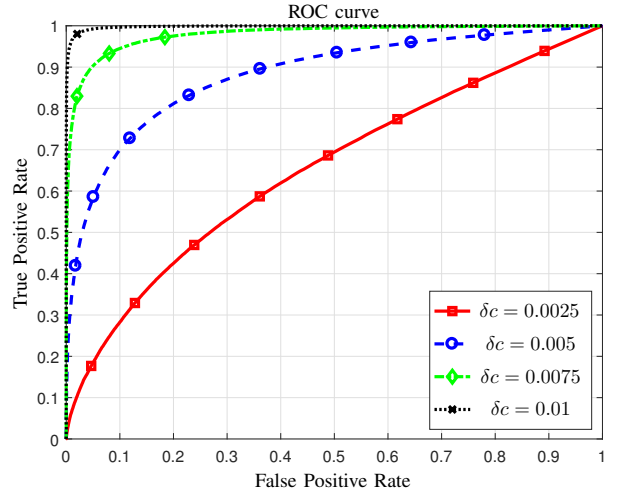


Fig. 7. ROC curve when testing for changes in the scale factor.

estimates were then derived as the solution to a constrained optimization problem. Further, we derived the EM recursions for estimating the model parameters that are needed for the optimization giving the MAP estimates, and described how to test for changes in the time-varying scale factor.

It was concluded that the FIM for the model with synchronous measurements is singular, and hence, that the CRB is unavailable. Consequently, we instead considered a similar model, where some of the inequality constraints originating from the OBD measurements are transformed into equality constraints. As expected, the resulting CRB indicated that the speed estimates will tend to improve at higher OBD resolutions and at lower GNSS error variances. Similarly, the scale factor estimates will tend to improve at higher OBD resolutions, at lower GNSS error variances, at higher speeds, and at lower scale factors. An experimental study was conducted by simulating measurements errors from real-world vehicle dynamics. The experiments aligned well with the CRB, and the proposed estimators were shown to provide a significantly better performance than can be achieved by

either of the sensors individually.

In summary, this paper has derived speed and scale factor estimators that exploit the complementary features of OBD and GNSS measurements of speed. The estimators are able to not only increase the estimation accuracy and the estimation rate, but also to strengthen the resilience to GNSS outages. Given the ubiquity of sensor setups utilizing OBD and GNSS measurements for insurance telematics and fleet management, the presented sensor fusion scheme can be expected to be of use in e.g., intelligent speed compliance and the detection of harsh braking. Further, it has been demonstrated that the estimation framework enables low-cost testing of changes in the scale factor. This could e.g., be used to provide tire-pressure monitoring as a value-added service in current telematics programs.

#### APPENDIX A

Here, we derive the EM iterations in (12). The expectation step consists of computing

$$Q(\boldsymbol{\theta}, \boldsymbol{\theta}^{(i)}) \triangleq \mathbb{E}_{p_{\boldsymbol{\theta}^{(i)}}(\mathbf{s}, c | \mathbf{s}^o, \mathbf{s}^g)}[\ln p_{\boldsymbol{\theta}}(\mathbf{s}, c, \mathbf{s}^o, \mathbf{s}^g)] \quad (19)$$

and the maximization step gives the updated estimates as [30]

$$\boldsymbol{\theta}^{(i+1)} = \arg \max_{\boldsymbol{\theta}} Q(\boldsymbol{\theta}, \boldsymbol{\theta}^{(i)}). \quad (20)$$

Now, note that  $\sigma_g^2$  and  $\sigma_s^2$  only alter the GNSS measurements and the prior, respectively, so that

$$\ln p_{\boldsymbol{\theta}}(\mathbf{s}, c, \mathbf{s}^o, \mathbf{s}^g) = \ln p_{\sigma_g^2}(\mathbf{s}^g | \mathbf{s}) + \ln p_{\sigma_s^2}(\mathbf{s}) + \ln p(\mathbf{s}^o | \mathbf{s}, c). \quad (21)$$

Hence, the updated estimates of  $\sigma_g^2$  and  $\sigma_s^2$  can be obtained as

$$\begin{aligned} \hat{\sigma}_{g,i+1}^2 &= \arg \max_{\sigma_g^2} \mathbb{E}_{p_{\boldsymbol{\theta}^{(i)}}(\mathbf{s} | \mathbf{s}^o, \mathbf{s}^g)}[\ln p_{\sigma_g^2}(\mathbf{s}^g | \mathbf{s})] \\ &= \arg \max_{\sigma_g^2} \sum_{k \in \mathcal{G}} \mathbb{E}_{p_{\boldsymbol{\theta}^{(i)}}(s_k | \mathbf{s}^o, \mathbf{s}^g)}[\ln p_{\sigma_g^2}(s_k^g | s_k)] \\ &= \arg \max_{\sigma_g^2} -\frac{1}{2\sigma_g^2} \sum_{k \in \mathcal{G}} \mathbb{E}_{p_{\boldsymbol{\theta}^{(i)}}(s_k | \mathbf{s}^o, \mathbf{s}^g)}[(s_k - s_k^g)^2] \\ &\quad - \frac{|\mathcal{G}|}{2} \ln \sigma_g^2 \end{aligned} \quad (22a)$$

and

$$\begin{aligned} \hat{\sigma}_{s,i+1}^2 &= \arg \max_{\sigma_s^2} \mathbb{E}_{p_{\boldsymbol{\theta}^{(i)}}(\mathbf{s} | \mathbf{s}^o, \mathbf{s}^g)}[\ln p_{\sigma_s^2}(\mathbf{s})] \\ &= \arg \max_{\sigma_s^2} \sum_{k=1}^{N-1} \mathbb{E}_{p_{\boldsymbol{\theta}^{(i)}}(s_k, s_{k+1} | \mathbf{s}^o, \mathbf{s}^g)}[\ln p_{\sigma_s^2}(s_{k+1} | s_k)] \\ &= \arg \max_{\sigma_s^2} -\frac{1}{2\sigma_s^2} \sum_{k=1}^{N-1} \frac{1}{\Delta t_k} \mathbb{E}_{p_{\boldsymbol{\theta}^{(i)}}(s_k, s_{k+1} | \mathbf{s}^o, \mathbf{s}^g)}[(s_{k+1} - s_k)^2] \\ &\quad - \frac{N-1}{2} \ln \sigma_s^2, \end{aligned} \quad (22b)$$

respectively. The EM recursions in (12) now immediately follow from (22).

#### APPENDIX B

This appendix will derive the inverse FIM in (17). We begin by writing the equality constraints from Section III-A as

$$\mathbf{g}(\mathbf{x}) = \mathbf{0}_{N-M,1} \quad (23)$$

where  $\mathbf{g}(\mathbf{x}) \triangleq c\mathbf{s}_{M+1:N} - \mathbf{s}_{M+1:N}^o - \boldsymbol{\gamma}_{M+1:N}$ , while  $\mathbf{s}_{M+1:N}^o$  and  $\boldsymbol{\gamma}_{M+1:N}$  are defined in analogy with  $\mathbf{s}_{M+1:N}$ . Moreover, the Jacobian of the constraints is

$$\mathbf{G} \triangleq \partial_{\mathbf{x}} \mathbf{g}(\mathbf{x}) = \begin{bmatrix} \mathbf{0}_{N-M,M} & c\mathbf{I}_{N-M} & \mathbf{s}_{M+1:N} \end{bmatrix} \quad (24)$$

and we can construct the matrix

$$\mathbf{U} \triangleq \begin{bmatrix} \mathbf{I}_M & \mathbf{0}_{M,1} \\ \mathbf{0}_{N-M+1,M} & \boldsymbol{\varphi} \end{bmatrix} \quad (25)$$

whose columns form a basis for the null space of  $\mathbf{G}$ . Now, noting that the FIM for the corresponding unconstrained problem (only considering the GNSS measurements) is

$$\mathcal{I} = \frac{1}{\sigma_g^2} \begin{bmatrix} \mathbf{I}_N & \mathbf{0}_{N,1} \\ \mathbf{0}_{1,N} & 0 \end{bmatrix}, \quad (26)$$

it follows that the inverse FIM, after including the equality constraints (23), becomes [31]

$$\mathbf{P} = \mathbf{U}(\mathbf{U}^T \mathcal{I} \mathbf{U})^{-1} \mathbf{U}^T \quad (27)$$

which gives (17) after straightforward calculations.

#### REFERENCES

- [1] J. Wahlström, I. Skog, and P. Händel, "Smartphone-based vehicle telematics — A ten-year anniversary," *IEEE Trans. Intell. Transport. Syst.*, vol. 18, no. 10, pp. 2802–2825, Oct. 2017.
- [2] J. Engelbrecht, M. J. Booysen, G.-J. van Rooyen, and F. J. Bruwer, "Survey of smartphone-based sensing in vehicles for intelligent transportation system applications," *IET Intell. Transport. Syst.*, vol. 9, no. 10, pp. 924–935, Dec. 2015.
- [3] "Smart transportation market by solution type (smart ticketing, parking management, passenger information, traffic management, integrated supervision, and insurance telematics), service, and region - Global forecast to 2021," Tech. Rep., Aug. 2017, Markets and markets, Report Code: TC 2365.
- [4] S. Kaplan, M. A. Guvensan, A. G. Yavuz, and Y. Karalurt, "Driver behavior analysis for safe driving: A survey," *IEEE Trans. Intell. Transport. Syst.*, vol. 16, no. 6, pp. 3017–3032, Dec. 2015.
- [5] "The state of usage based insurance today," Jun. 2016, Ptolemus - Consulting Group.
- [6] A. Chowdhury, T. Chakravarty, and P. Balamuralidhar, "Estimating true speed of moving vehicle using smartphone-based GPS measurement," in *Proc. IEEE Int. Conf. Syst., Man Cybernetics*, San Diego, CA, Oct. 2014, pp. 3348–3353.
- [7] G. Andria, F. Attivissimo, A. D. Nisio, A. M. L. Lanzolla, and A. Pellegrino, "Design and implementation of automotive data acquisition platform," in *Proc. IEEE Int. Instrum. Meas. Technol.*, Pisa, Italy, May 2015, pp. 272–277.
- [8] X. Niu, Q. Wang, Y. Li, Q. Li, and J. Liu, "Using inertial sensors in smartphones for curriculum experiments of inertial navigation technology," *Educ. Sci.*, vol. 5, no. 1, pp. 26–46, Mar. 2015.
- [9] J. Xu, H. He, F. Qin, and L. Chang, "A novel autonomous initial alignment method for strapdown inertial navigation system," *IEEE Trans. Instrum. Meas.*, vol. 66, no. 9, pp. 2274–2282, Sep. 2017.
- [10] P. Händel, I. Skog, J. Wahlström, F. Bonawiede, R. Welch, J. Ohlsson, and M. Ohlsson, "Insurance telematics: Opportunities and challenges with the smartphone solution," *IEEE Intell. Transport. Syst. Mag.*, vol. 6, no. 4, pp. 57–70, Oct. 2014.
- [11] J. Wahlström, I. Skog, and P. Händel, "IMU alignment for smartphone-based automotive navigation," in *Proc. 18th IEEE Int. Conf. Inf. Fusion*, Washington, DC, Jul. 2015, pp. 1437–1443.



- [12] J. Wahlström, I. Skog, and P. Händel, "Driving behavior analysis for smartphone-based insurance telematics," in *Proc. 2nd Workshop on Physical Analytics*, Florence, Italy, May 2015, pp. 19–24.
- [13] N. El-Sheimy, K. W. Chiang, and A. Noureldin, "The utilization of artificial neural networks for multisensor system integration in navigation and positioning instruments," *IEEE Trans. Instrum. Meas.*, vol. 55, no. 5, pp. 1606–1615, Oct. 2006.
- [14] C. Thompson, J. White, B. Dougherty, A. Albright, and D. Schmidt, "Using smartphones to detect car accidents and provide situational awareness to emergency responders," in *Mobile Wireless Middleware, Operating Syst., Appl.* Springer, Jun. 2010, vol. 48, pp. 29–42.
- [15] A. E. Kubba and K. Jiang, "A comprehensive study on technologies of tyre monitoring systems and possible energy solutions," *Sensors*, vol. 14, no. 6, pp. 10 306–10 345, Jun. 2014.
- [16] S. Velupillai and L. Guvenc, "Tire pressure monitoring," *IEEE Control Syst.*, vol. 27, no. 6, pp. 22–25, Dec. 2007.
- [17] S. Gaglione and M. Petovello, "How does a GNSS receiver estimate velocity?" *insideGNSS*, vol. 10, no. 2, pp. 38–41, Mar. 2015.
- [18] D. I. Katzourakis, E. Velenis, D. Abbink, R. Happee, and E. Holweg, "Race-car instrumentation for driving behavior studies," *IEEE Trans. Instrum. Meas.*, vol. 61, no. 2, pp. 462–474, Feb. 2012.
- [19] P. D. Groves, *Principles of GNSS, inertial, and multisensor integrated navigation systems*, 1st ed. Artech House, 2008.
- [20] "Global OBD vehicle communication software manual," Snap-on, Tech. Rep., Aug. 2013.
- [21] F. Gustafsson, "Rotational speed sensors: Limitations, pre-processing and automotive applications," *IEEE Trans. Instrum. Meas.*, vol. 13, no. 2, pp. 16–23, Apr. 2010.
- [22] M. Matosevic, Z. Salcic, and S. Berber, "A comparison of accuracy using a GPS and a low-cost DGPS," *IEEE Trans. Instrum. Meas.*, vol. 55, no. 5, pp. 1677–1683, Oct. 2006.
- [23] A. Forsgren, P. E. Gill, and M. H. Wright, "Interior methods for nonlinear optimization," *SIAM Rev.*, vol. 44, no. 4, pp. 525–597, Apr. 2002.
- [24] G. Wei, G. C., and M. A. Tanner, "A Monte Carlo implementation of the EM algorithm and the poor man's data augmentation algorithms," *J. American Statistical Association*, vol. 85, no. 411, pp. 699–704, Sep. 1990.
- [25] S. M. Kay, *Fundamentals of Statistical Signal Processing: Detection Theory*. Prentice-Hall, 1998.
- [26] S. L. Miller, B. Youngberg, A. Millie, P. Schweizer, and C. Gerdes, "Calculating longitudinal wheel slip and tire parameters using GPS velocity," in *Proc. Int. Conf. American Controls*, Arlington, VA, Jun. 2001, pp. 1800–1805.
- [27] S. M. Kay, *Fundamentals of Statistical Signal Processing: Estimation Theory*. Prentice-Hall, 1993.
- [28] T. J. Moore, "A theory of Cramér-Rao bounds for constrained parametric models," Ph.D. dissertation, University of Maryland, 2010.
- [29] DoD, "NAVSTAR GPS - User equipment introduction," US Department of Defense, Public Release Version, Tech. Rep., Sep. 1996.
- [30] T. B. Schön, "An explanation of the expectation maximization algorithm," Linköping University, Tech. Rep., Aug. 2009.
- [31] T. J. Moore and B. M. Sadler, "The value of information in constrained parametric models," in *Proc. IEEE Statistical Signal Process. Workshop*, Ann Arbor, MI, Aug. 2012, pp. 293–296.



**Johan Wahlström** received his MSc degree in Engineering Physics and PhD degree in Electrical Engineering from KTH Royal Institute of Technology, Stockholm, Sweden, in 2014 and 2017, respectively. His main PhD research topic was smartphone-based automotive navigation. In 2015, he received a scholarship from the Sweden-America foundation and spent six months at Washington University, St. Louis, USA. In the fall of 2016, he did a six-week internship at Cambridge Mobile Telematics. Since January 2018, he is a postdoc at Oxford University.



**Isaac Skog** (S'09-M'10) received the BSc and MSc degrees in Electrical Engineering from the KTH Royal Institute of Technology, Stockholm, Sweden, in 2003 and 2005, respectively. In 2010, he received the Ph.D. degree in Signal Processing with a thesis on low-cost navigation systems. In 2009, he spent 5 months at the Mobile Multi-Sensor System research team, University of Calgary, Canada, as a visiting scholar and in 2011 he spent 4 months at the Indian Institute of Science (IISc), Bangalore, India, as a visiting scholar. He is currently a Researcher at KTH coordinating the KTH Insurance Telematics Lab. He was a recipient of a Best Survey Paper Award by the IEEE Intelligent Transportation Systems Society in 2013.



stationary satellites.

**Robin Larsson** received the MSc degree in Engineering Physics from KTH in 2005. In 2014, Robin joined the Signal Processing Lab as a part time PhD student, advised by Isaac Skog. Robin is on part time study leave from his position at OHB-Sweden as AOCs (Attitude and Orbit Control Systems) Specialist. He joined the space division of Swedish Space Corporation in 2005, which in 2011 became OHB-Sweden. The main focus of his work has been GNC (Guidance, Navigation and Control) for formation flying of satellites, and AOCs for geo-



**Peter Händel** (S'88-M'94-SM'98) received a Ph.D. degree from Uppsala University, Uppsala, Sweden, in 1993. From 1987 to 1993, he was with Uppsala University. From 1993 to 1997, he was with Ericsson AB, Kista, Sweden. From 1996 to 1997, he was a Visiting Scholar with the Tampere University of Technology, Tampere, Finland. Since 1997, he has been with the KTH Royal Institute of Technology, Stockholm, Sweden, where he is currently a Professor of Signal Processing. From 2000 to 2006, he held an adjunct position at the Swedish Defence Research Agency. He has been a Guest Professor at the Indian Institute of Science (IISc), Bangalore, India, and at the University of Gävle, Sweden. He is a co-founder of Movelo AB. Dr. Händel has served as an associate editor for the IEEE TRANSACTIONS ON SIGNAL PROCESSING. He was a recipient of a Best Survey Paper Award by the IEEE Intelligent Transportation Systems Society in 2013.